Chapter 2

Methodology

2.1 Introduction

In the last few decades, various transport models have been put forward to probe nuclear dynamics at different incident energies. This is because of the fact that all experimental measurements are done when matter is cold and fragmented. No experimental measurement can gauge the phase of high density and temperature. Therefore, one needs reliable transport model which is capable of following the reaction from the start when nuclei are well separated to the end when matter is cold and fragmented. Many theoretical approaches that can characterize various aspects of a reaction have been reported in the literature. Unfortunately, no single model is able to explain all characteristics of a reaction completely.

As stated in the previous chapter, ordinary mean field theory [190, 191] similar to that of Hatree-Fock and Schrödinger equation is best suited to explain the reaction mechanism at lower tail of the energy. The Time-Dependent Hatree-Fock (TDHF) theory [167] takes into account the time evolution of many-fermionic system and is an approximation of the time-dependent Schrödinger equation with the use of a single Slater determinant. This theory yielded good results for the system propagating under the influence of mean field alone whereas, at the same time, it was found to be very difficult to use it for the large scale investigations in heavy-ion collisions at intermediate energies. This happens because of the fact that at intermediate energies, frequent nucleon-nucleon (NN) collisions dominate the reaction [192]. But at the other extreme, the *Cascade model* [193] is convenient to study the heavy-ion collisions at ultra high incident energies. The transport model based on the one-body or many-body correlations can explain dynamics at intermediate energies

nicely. In the next section, we will discuss some of these methods.

2.1.1 The intranuclear cascade (INC) model

It is worth mentioning that the mean field is completely ignored in the INC model and nucleon-nucleon (NN) collisions are taken explicitly without considering Pauli-blocking into account. Due to the absence of mean field, nucleons proceed in a straight line trajectories between any two binary collisions. Here, each nucleon is taken as a bunch of point particles; distributed within a sphere of radius $R = R_0 A^{1/3}$ (where 'A' is the mass of either nucleus); using the *Monte-Carlo Sampling* in the absence of Fermi-momentum (that must be assign in principle, to each nucleus). The *Cascade* is a very fast process (takes place in about 10^{-22} seconds and is based on the assumption that incoming particles interact with individual nucleons of the target. This model is consistent in gathering information regarding different experimental observables [194] at high incident energies. But if we look for the observables at intermediate energies (for example, the collective flow and the multifragmentation), these are very sensitive to the initial Fermi-momentum distribution of the nucleons as well as to the intrinsic pressure that comes up due to the mean field during a reaction. Due to these drawbacks, the scope of the INC model is limited to high energy heavy-ion collisions only where the effect of mean field can safely be assumed to be insignificant. These limitations were then removed later on by Cugnon *et al.* [195], who developed a *Monte-Carlo* method that incorporates compression and decomposition effects (which were ignored in the original INC model). These effects are required to study the observables like collective flow, multifragmentation etc. But again, the absence of mean field potential makes it unsuitable for studying the phenomena like multifragmentation. Thus, from time to time, efforts have been made in the literature to improve the original INC approach by incorporating various features that include e.g.,

- initial positions of the nucleons in target/projectile are chosen randomly in the sphere of radius $R = 1.18\ A^{1/3}$ with a sharp surface;

- the use of relativistic kinematics;

- initial momenta are generated by distributing nucleons as a Fermi-gas inside the square well potential;

- the Pauli principle is enforced by using statistical blocking factors etc. to extend its validity to lower incident energies [196] and;

- introducing the isospin degree of freedom for all types of particles.

In this direction, the demand of both mean field and binary NN collisions in the theoretical approaches have been put forward to study the dynamics of nuclear matter at intermediate energy heavy-ion collisions. A correct information about the real and imaginary parts of the potential is required for better understanding of the nuclear dynamics. Both these factors influence the dynamics (as real part influences the trajectory of the nucleons whereas imaginary part deals with the NN collisions). Therefore, next we shall discuss various transport models that can be used to describe reaction dynamics at intermediate energies where various phenomena such as collective flow, multifragmentation, nuclear stopping and subthreshold particle production etc. come into picture. The transport models used at intermediate energies can broadly be divided into two categories:

1. dynamical models (like VUU and IBUU) that follow the time evolution of one-body phase space distribution and;

2. dynamical models based on $\acute{N}$-body molecular dynamics or *Cascade* schemes i.e., QMD and IQMD models. In this chapter, we will describe the QMD and IQMD models in detail because the present study is planned to be carried out using IQMD model.

The failure of one-body models [4, 20, 197] in explaining many-body observables created the need of many-body models. In the following sections, we will describe, in detail, the $\acute{N}$-body molecular dynamics approaches [4, 20, 35, 170, 198–201].

Hence firstly, we shall give an overview of the models that explain the reaction mechanism without taking isospin effects into account. Later, various theoretical models that can explain the reaction dynamics with isospin effects shall be discussed. These models help to explain the essential isospin physics that governs the complex nuclear matter interactions among the neutrons and protons (particles with different charge states interacting inside reaction zone).

2.2 Various models used to investigate the heavy-ion collisions without isospin effects

Here, we will discuss many-body molecular dynamics approaches (without isospin effects) [35, 169, 171–174, 176–178, 180–183, 189]. In particular, standard Quantum Molecular Dynamics (QMD) model [35] (which is an $\acute{N}$-body model) will be described in detail along with an overview of various modifications/extensions of the model.

2.2.1 Quantum Molecular Dynamics model

The Quantum Molecular Dynamics (QMD) approach [35] is one of the many body ($\acute{N}$-body) molecular dynamics approaches. The Classical Molecular Dynamics (CMD) approach [169] was the first $\acute{N}$-body approach that covered compression as well as fragment formation in classical picture. It incorporates Hamilton's equations of motion along with the finite range nucleon-nucleon potential. Keeping the CMD approach as a base and incorporating $\acute{N}$-body correlations, an equation of state and most important, various quantum effects (such as the Pauli-potential, Stochastic scattering as well as particle production), Aichelin and Stöcker developed new model in late 1980's, and this model was dubbed as "Quantum Molecular Dynamics" (QMD) model. This model simulates the intermediate energy heavy-ion collisions on an event by event basis, taking all the fluctuations and correlations into account.

Each transport model follows three layer procedure to simulate a reaction. The very first step is to generate both target and projectile. This procedure is termed as *initialization*. It is also necessary to check if initialization doesn't destabilize the cold nuclei. For this, some initial checks for the stability of nuclei (i.e., projectile/target) should be carried out. After the successful initialization, the projectile and target are allowed to propagate under the effect of surrounding mean field and this process is known as *propagation*. Finally, nucleons are bound to scatter (elastically or inelastically) if they come too close to each other and this procedure is dubbed as *nucleon-nucleon collisions*. This is further subjected to the fulfilment of the Pauli-principle. Now, we shall give details of each of the above mentioned steps (i.e., *initialization*, *propagation* and *nucleon-nucleon collisions*) one by one.

2.2.2 Initialization

For the process of initialization of a nucleus in QMD model, one has to first assign coordinates and momenta to each nucleon of the nucleus. Therefore, we determine the positions of each nucleon in a sphere with radius, R = $1.14A^{1/3}$ (where 'A' stands for the mass of either nucleus) with the help of *Monte-Carlo* method. The coordinates of nucleons are rejected if their distance is less than 1.5 fm. The local densities at the centers of all the nucleons are determined by all other fellow nucleons. With the help of local Fermi-gas approximation, the local Fermi-momentum is calculated by using the relation

$$\mathbf{P}_F(\mathbf{r}_i) = \sqrt{-2mU(\mathbf{r}_i)}, \tag{2.1}$$

where, $U(\mathbf{r}_i)$ is the local potential. The momenta of all nucleons are chosen randomly between zero and $\mathbf{P}_F$. We reject all those distributions where two nucleons are closer than a minimum distance d_{min}. In other words, we require

$$(\mathbf{r}_i - \mathbf{r}_j)^2(\mathbf{p}_i - \mathbf{p}_j)^2 \geq d_{min}. \tag{2.2}$$

In the QMD model, the nucleons are expressed as Gaussian wave packets which interact via mutual two- and three-body interactions. Here, wavefunction of each nucleon is illustrated as a wavepacket with width $\sqrt{L}$ centered around $\mathbf{r}_i(t)$ and $\mathbf{p}_i(t)$:

$$\psi_i(\mathbf{r}, \mathbf{p}_i(t), \mathbf{r}_i(t)) = \frac{1}{(2\pi L)^{3/4}} e^{\left[\frac{i}{\hbar}\mathbf{p}_i(t)\cdot\mathbf{r} - \frac{(\mathbf{r}-\mathbf{r}_i(t))^2}{4L}\right]}. \tag{2.3}$$

To get the detailed explanation on the parameter 'L', see Refs. [35, 189]. The total $\acute{N}$-body function is assumed to be a direct product of the coherent states:

$$\Phi = \prod_i \psi_i(\mathbf{r}, \mathbf{r}_i, \mathbf{p}_i, t). \tag{2.4}$$

In the QMD model, anti-symmetrization of the wave function is not taken into consideration because this model doesn't use the *Slater determinant* summation. It is well known that the dynamics due to the real part of the nucleon-nucleon interaction was tested by comparing the calculations of the QMD model with explicitly suppressed collision term to the solution of the TDHF and *Vlasov equation* [35, 202]. The resemblance of the time evolution in all three approaches led to the conclusion that both detailed form of the wave function of the TDHF approach as well as width of the Gaussian [35, 203] do not

play significant role in determining the time evolution [35, 202] provided it fulfils the minimal requirements like the approximate constant density over the proper region in the coordinate space as well as binding energy of each nucleus etc. [35].

Since, the QMD model is a semi-classical approach, therefore, in order to traverse from quantum mechanical wave function to classical distribution function in phase space, the Wigner distribution function is used. The Wigner transform of the rational states are the Gaussians in coordinate and momentum space that obey uncertainty principle [35]. The Wigner density is given as:

$$
\begin{aligned}
f_i(\mathbf{r},\mathbf{p},\mathbf{r}_i(t),\mathbf{p}_i(t)) &= \frac{1}{(2\pi\hbar)^3}\int e^{-\frac{i}{\hbar}\mathbf{p}\cdot\mathbf{r}_{12}}\psi_i(\mathbf{r}+\frac{\mathbf{r}_{12}}{2},t)\psi_i^*(\mathbf{r}-\frac{\mathbf{r}_{12}}{2},t)d^3r_{12},\\
&= \frac{1}{(2\pi\hbar)^3}\frac{1}{(2\pi L)^{3/2}}\int e^{-\frac{i}{\hbar}\mathbf{p}\cdot\mathbf{r}_{12}}e^{\frac{i}{\hbar}\mathbf{p}_i(t)\cdot(\mathbf{r}+\frac{\mathbf{r}_{12}}{2})-\frac{[\mathbf{r}+\frac{\mathbf{r}_{12}}{2}-\mathbf{r}_i(t)]^2}{4L}}\\
&\qquad\qquad \times e^{-\frac{i}{\hbar}\mathbf{p}_i(t)\cdot(\mathbf{r}-\frac{\mathbf{r}_{12}}{2})-\frac{[\mathbf{r}-\frac{\mathbf{r}_{12}}{2}-\mathbf{r}_i(t)]^2}{4L}}d^3r_{12},\\
&= \frac{1}{(2\pi\hbar)^3}\frac{1}{(2\pi L)^{3/2}}\int e^{-\frac{i}{\hbar}\mathbf{p}\cdot\mathbf{r}_{12}}e^{\frac{i}{\hbar}\mathbf{p}_i(t)\cdot\mathbf{r}_{12}-(\mathbf{r}-\mathbf{r}_i(t))^2/2L-\mathbf{r}_{12}^2/8L}d^3r_{12},\\
&= \frac{1}{(2\pi\hbar)^3}\frac{1}{(2\pi L)^{3/2}}\int e^{-\frac{i}{\hbar}(\mathbf{p}-\mathbf{p}_i(t))^2\cdot\mathbf{r}_{12}}e^{-(\mathbf{r}-\mathbf{r}_i(t))^2/2L-\mathbf{r}_{12}^2/8L}d^3r_{12},\\
&= \frac{1}{(2\pi\hbar)^3}\frac{1}{(2\pi L)^{3/2}}e^{-(\mathbf{r}-\mathbf{r}_i(t))^2/2L}\int e^{-\frac{i}{\hbar}(\mathbf{p}-\mathbf{p}_i(t))^2\cdot\mathbf{r}_{12}-\mathbf{r}_{12}^2/8L}d^3r_{12},\\
&= \frac{1}{(2\pi\hbar)^3}\frac{1}{(2\pi L)^{3/2}}e^{-(\mathbf{r}-\mathbf{r}_i(t))^2/2L}\\
&\quad\times\int e^{-\left[\frac{i}{\hbar}(\mathbf{p}-\mathbf{p}_i(t))^2\cdot\mathbf{r}_{12}+\mathbf{r}_{12}^2/8L+i^2(\mathbf{p}-\mathbf{p}_i(t))^2 2L/\hbar^2-i^2(\mathbf{p}-\mathbf{p}_i(t))^2 2L/\hbar^2\right]}d^3r_{12},\\
&= \frac{1}{(2\pi\hbar)^3}\frac{1}{(2\pi L)^{3/2}}e^{-(\mathbf{r}-\mathbf{r}_i(t))^2/2L}e^{-(\mathbf{p}-\mathbf{p}_i(t))^2 2L/\hbar^2}\\
&\quad\times\int e^{-\left[\frac{i}{\hbar}(\mathbf{p}-\mathbf{p}_i(t))\sqrt{2L}+\mathbf{r}_{12}/2\sqrt{2L}\right]^2}d^3r_{12},\\
&= \frac{1}{(2\pi\hbar)^3}\frac{1}{(2\pi L)^{3/2}}e^{-(\mathbf{r}-\mathbf{r}_i(t))^2/2L}e^{-(\mathbf{p}-\mathbf{p}_i(t))^2 2L/\hbar^2}\times\left(2\sqrt{2\pi L}\right)^3,\\
&= \frac{1}{(\pi\hbar)^3}e^{-(\mathbf{r}-\mathbf{r}_i(t))^2/2L}e^{-(\mathbf{p}-\mathbf{p}_i(t))^2 2L/\hbar^2}. \qquad (2.5)
\end{aligned}
$$

Here, $\mathbf{r}_i(t)$ and $\mathbf{p}_i(t)$ are the centroids of Gaussian wave packet in phase space. It is worth

mentioning that, the value of 'L' is kept fixed. The density of i^{th} particle is given by:

$$\begin{aligned}
\rho_i(\mathbf{r}) &= \int f_i(\mathbf{r},\mathbf{p},\mathbf{r}_i(t),\mathbf{p}_i(t))d^3p, \\
&= \int \frac{1}{(\pi\hbar)^3} e^{-[\mathbf{r}-\mathbf{r}_i(t)]^2/2L} e^{-[\mathbf{p}-\mathbf{p}_i(t)]^2 2L/\hbar^2} d^3p, \\
&= \frac{1}{(\pi\hbar)^3} e^{-[\mathbf{r}-\mathbf{r}_i(t)]^2/2L} \int e^{-[\mathbf{p}-\mathbf{p}_i(t)]^2 2L/\hbar^2} d^3p, \\
&= \frac{1}{(\pi\hbar)^3} e^{-[\mathbf{r}-\mathbf{r}_i(t)]^2/2L} \left[(\sqrt{\frac{\pi\hbar^2}{2L}} \right)^3, \\
&= \frac{1}{(2\pi L)^{3/2}} e^{-[\mathbf{r}-\mathbf{r}_i(t)]^2/2L}. \qquad (2.6)
\end{aligned}$$

As stated above, we have to first assign coordinates and momentum to each nucleon. In three dimensional space (inside a sphere of radius $R = 1.14A^{1/3}$), the centroid of Gaussian wave packet is uniformly distributed in polar coordinates by the relation

$$\begin{aligned}
\mathbf{r} &= R\ a_1^{1/3}, \\
cos\ \theta_1 &= 1 - 2\ a_2, \\
\phi_2 &= 2\pi\ a_3, \qquad (2.7)
\end{aligned}$$

where, a_1, a_2 and a_3 are the random numbers.

Further, the center of each Gaussian wave packet in momentum space is uniformly distributed in polar coordinates by

$$\begin{aligned}
\mathbf{p}_i &= \mathbf{P}_F(\mathbf{r}_i)\ a_4^{1/3}, \\
cos\ \theta_{11} &= 1 - 2\ a_5, \\
\phi_{12} &= 2\pi\ a_6, \qquad (2.8)
\end{aligned}$$

where, a_4, a_5 and a_6 are again the random numbers.

Therefore, under the present conditions (as discussed above), a very large number of initializations are rejected. All eigen states of a Hamiltonian should follow the uncertainty relation. Each level occupies a volume of 'h' in the phase space. Also, in the ground state of the system, the phase space is densely filled up to the highest level in coordinate and momentum space without any vacancy. This property of the ground state helps to initialize the nuclei and normally, it takes thousands of initializations to generate one proper nucleus. The above initial phase space distribution is consistent with the experiments as

well as with the theoretical calculations of PPW + RPA (Pandharipande, Papanicolas and Wambach + Random Phase Approximation) approach [4, 20]. This complete process of initialization leads to the the proper root mean square (r.m.s.) radii in both coordinate and momentum spaces [35]. The stability of each nuclei was also looked carefully by the *Frankfurt group* [204]. They put forward that the inclusion of Pauli-potential in the mean field increases the stability of a nucleus for longer time. In this direction, *Nantes group* [35] also checked the stability with the help of root mean square radii as well as binding energy. Most of the nuclei were found to be stable for couple of hundred fm/c; which is long enough for the present purpose.

2.2.3 Propagation

In this step, successfully initialized nuclei i.e., projectile and target generated with proper initializations are boosted towards each other with proper center of mass velocity. The equation of motion of many-body system is, then, calculated using generalized variational principle; we start from the action

$$S = \int_{t_1}^{t_2} \mathcal{L}[\Phi, \Phi^*]dt, \tag{2.9}$$

where, Lagrange function is given as:

$$\mathcal{L} = \langle \Phi | i\hbar \frac{d}{dt} - H | \Phi \rangle, \tag{2.10}$$

here, the total time derivatives include the derivation with respect to the parameters. To obtain the time evolution, the action is assumed to be stationary under the allowed variation of the wave function, i.e.,

$$\delta S = \delta \int_{t_1}^{t_2} \mathcal{L}[\Phi, \Phi^*]dt = 0. \tag{2.11}$$

Since under allowed variation of the wave function, the action is assumed to be stationary and therefore, this yields an Euler-Lagrange equation for each parameter λ, which reads as:

$$\frac{d}{dt}\frac{\partial \mathcal{L}}{\partial \dot{\lambda}} - \frac{\partial \mathcal{L}}{\partial \lambda} = 0. \tag{2.12}$$

If the true solution of the Schrödinger equation is contained in the restricted set of wave function $\psi_i(\mathbf{r}, \mathbf{r}_i(\mathrm{t}), \mathbf{p}_i(\mathrm{t}))$, this variation of the action will give the exact solution of the Schröndiger equation.

For the rational states and Hamiltonian comprising of kinetic term T_i and mutual interactions V_{ij}; which can be described as the real part of the Brückner G matrix augmented by the Coulomb interaction, the Lagrangian and the variation can easily be calculated and we obtain:

$$\mathcal{L} = \sum_i \left[-\dot{\mathbf{r}}_i \mathbf{p}_i - T_i - \frac{1}{2} \sum_{j \neq i} \langle V_{ij} \rangle - \frac{3}{2Lm} \right], \tag{2.13}$$

$$\dot{\mathbf{r}}_i = \frac{\mathbf{p}_i}{m} + \nabla_{\mathbf{p}_i} \sum_j \langle V_{ij} \rangle = \nabla_{\mathbf{p}_i} \langle H \rangle, \tag{2.14}$$

$$\dot{\mathbf{p}}_i = -\nabla_{\mathbf{r}_i} \sum_{j \neq i} \langle V_{ij} \rangle = -\nabla_{\mathbf{r}_i} \langle H \rangle, \tag{2.15}$$

with $\mathbf{r}_i = \mathbf{r}_i + \frac{\mathbf{p}_i}{m} t$ and $\langle V_{ij} \rangle = \int d^3\mathbf{r}_1 d^3\mathbf{r}_2 \langle \psi_i^* \psi_j^* | V(\mathbf{r}_1, \mathbf{r}_2) | \psi_i \psi_j \rangle$. The time evolution of $\acute{N}$-body Schrödinger equation can be reduced to the time evolution $6 \times (A_{tot})$ differential equations, by employing the variational principle, which can be solved numerically. The equations of motion are similar to the classical Hamilton equations i.e.,

$$\dot{\mathbf{p}}_i = -\frac{\partial \langle H \rangle}{\partial \mathbf{r}_i}; \qquad \dot{\mathbf{r}}_i = \frac{\partial \langle H \rangle}{\partial \mathbf{p}_i}. \tag{2.16}$$

The numerical solution can be achieved in the spirit of the classical molecular dynamics [205–207]. The expectation value of the total Hamiltonian is given as:

$$\begin{aligned} \langle H \rangle &= \langle T \rangle + \langle V \rangle \\ &= \sum_i \frac{p_i^2}{2m_i} + V^{Sky} + V^{Yuk} + V^{Coul} + V^{MDI}. \end{aligned} \tag{2.17}$$

Here, V^{Sky}, V^{Yuk}, V^{Coul} and V^{MDI} represent the local (two- and three-body) Skyrme, Yukawa, Coulomb and momentum-dependent potentials, respectively. The local Skyrme interaction is given by:

$$V^{Sky} = \frac{1}{2!} \sum_{j;i \neq j} V_{ij}^{(2)} + \frac{1}{3!} \sum_{j,k;i \neq j \neq k} V_{ijk}^{(3)}. \tag{2.18}$$

Here, $V_{ij}^{(2)}$ and $V_{ijk}^{(3)}$ represent the two- and three-body parts of the Skyrme interactions, respectively. The two-body interactions $V_{ij}^{(2)}$ are obtained by folding the two-body potential

with the densities of both the nucleons.

$$
\begin{aligned}
\sum_{j;i\neq j} V_{ij}^{(2)} &= \sum_{j;i\neq j} \int f_i(\mathbf{r}_i,\mathbf{p}_i,t) f_j(\mathbf{r}_j,\mathbf{p}_j,t) V(\mathbf{r}_i,\mathbf{r}_j) \\
&\quad \times d^3r_i d^3r_j d^3p_i d^3p_j, \\
&= \sum_{j;i\neq j} \int f_i(\mathbf{r}_i,\mathbf{p}_i,t) f_j(\mathbf{r}_j,\mathbf{p}_j,t) t_1 \\
&\quad \times \delta(\mathbf{r}_i-\mathbf{r}_j) d^3r_i d^3r_j d^3p_i d^3p_j, \\
&= \sum_{j;i\neq j} t_1 \int f_i(\mathbf{r}_i,\mathbf{p}_i,t) f_j(\mathbf{r}_j,\mathbf{p}_j,t) \\
&\quad \times d^3r d^3p_i d^3p_j, \\
&= \sum_{j;i\neq j} t_1 \int \frac{1}{(\pi\hbar)^3} e^{-(\mathbf{r}-\mathbf{r}_i(t))^2/2L} e^{-(\mathbf{p}-\mathbf{p}_i(t))^2 2L/\hbar^2} \\
&\quad \times \frac{1}{(\pi\hbar)^3} e^{-(\mathbf{r}-\mathbf{r}_j(t))^2/2L} e^{-(\mathbf{p}-\mathbf{p}_j(t))^2 2L/\hbar^2} d^3r d^3p_i d^3p_j, \\
&= \frac{1}{(\pi\hbar)^6} \left(\sqrt{\frac{\pi\hbar^2}{2L}}\right)^3 \left(\sqrt{\frac{\pi\hbar^2}{2L}}\right)^3 \sum_{j;i\neq j} t_1 \int e^{-(\mathbf{r}-\mathbf{r}_i(t))^2/2L} e^{-(\mathbf{r}-\mathbf{r}_j(t))^2/2L} d^3r, \\
&= \frac{1}{(2\pi L)^3} \sum_{j;i\neq j} t_1 \int e^{-(\mathbf{r}-\mathbf{r}_i(t))^2/2L-(\mathbf{r}-\mathbf{r}_j(t))^2/2L} d^3r, \\
&= \frac{1}{(2\pi L)^3} \sum_{j;i\neq j} t_1 \int e^{-\left[\frac{\mathbf{r}^2}{L}-\frac{\mathbf{r}}{L}(\mathbf{r}_i+\mathbf{r}_j)\right]-\left(\frac{\mathbf{r}_i^2+\mathbf{r}_j^2}{2L}\right)} d^3r, \\
&= \frac{1}{(2\pi L)^3} \sum_{j;i\neq j} t_1 \int e^{-\left[\left\{\frac{\mathbf{r}^2}{L}-\frac{\mathbf{r}}{L}(\mathbf{r}_i+\mathbf{r}_j)+\left(\frac{\mathbf{r}_i+\mathbf{r}_j}{2\sqrt{L}}\right)^2\right\}-\left(\frac{\mathbf{r}_i+\mathbf{r}_j}{2\sqrt{L}}\right)^2\right]} e^{-\left(\frac{\mathbf{r}_i^2+\mathbf{r}_j^2}{2L}\right)} d^3r, \\
&= \frac{1}{(2\pi L)^3} \sum_{j;i\neq j} t_1 \int e^{-\left[\left\{\frac{\mathbf{r}}{\sqrt{L}}-\left(\frac{\mathbf{r}_i+\mathbf{r}_j}{2\sqrt{L}}\right)\right\}^2-\left(\frac{\mathbf{r}_i+\mathbf{r}_j}{2\sqrt{L}}\right)^2\right]} e^{-\left(\frac{\mathbf{r}_i^2+\mathbf{r}_j^2}{2L}\right)} d^3r, \\
&= \frac{1}{(2\pi L)^3} \sum_{j;i\neq j} t_1 \int e^{-\left[\left\{\frac{\mathbf{r}}{\sqrt{L}}-\left(\frac{\mathbf{r}_i+\mathbf{r}_j}{2\sqrt{L}}\right)\right\}^2-\left(\frac{\mathbf{r}_i^2}{4L}+\frac{\mathbf{r}_j^2}{4L}+\frac{\mathbf{r}_i\mathbf{r}_j}{2L}\right)+\left(\frac{\mathbf{r}_i^2}{2L}+\frac{\mathbf{r}_j^2}{2L}\right)\right]} d^3r, \\
&= \frac{1}{(2\pi L)^3} \sum_{j;i\neq j} t_1 \int e^{-\left[\left\{\frac{\mathbf{r}}{\sqrt{L}}-\left(\frac{\mathbf{r}_i+\mathbf{r}_j}{2\sqrt{L}}\right)\right\}^2+\left(\frac{\mathbf{r}_i^2}{4L}+\frac{\mathbf{r}_j^2}{4L}-\frac{\mathbf{r}_i\mathbf{r}_j}{2L}\right)\right]} d^3r, \\
&= \frac{1}{(2\pi L)^3} \sum_{j;i\neq j} t_1 \int e^{-\left[\left\{\frac{\mathbf{r}}{\sqrt{L}}-\left(\frac{\mathbf{r}_i+\mathbf{r}_j}{2\sqrt{L}}\right)\right\}^2+\left(\frac{\mathbf{r}_i}{2\sqrt{L}}-\frac{\mathbf{r}_j}{2\sqrt{L}}\right)^2\right]} d^3r,
\end{aligned}
$$

$$
\begin{aligned}
&= \frac{1}{(2\pi L)^3}\sum_{j;i\neq j} t_1 e^{-(\mathbf{r}_i-\mathbf{r}_j)^2/4L}\int e^{-\left\{\frac{\mathbf{r}}{\sqrt{L}}-\left(\frac{\mathbf{r}_i+\mathbf{r}_j}{2\sqrt{L}}\right)\right\}^2} d^3r,\\
&= \sum_{j;i\neq j} t_1 e^{-(\mathbf{r}_i-\mathbf{r}_j)^2/4L}\ \ \frac{1}{(2\pi L)^3}\ \ (\sqrt{\pi L})^3,\\
&= \sum_{j} t_1 \frac{1}{(4\pi L)^{3/2}} e^{-(\mathbf{r}_i-\mathbf{r}_j)^2/4L},\\
&= t_1\sum_{j;i\neq j}\rho_{ij}, \qquad (2.19)
\end{aligned}
$$

where,

$$\rho_{ij} = \int d^3r\rho_i(\mathbf{r})\rho_j(\mathbf{r}) = \frac{1}{(4\pi L)^{3/2}} e^{-(\mathbf{r}_i-\mathbf{r}_j)^2/4L}. \qquad (2.20)$$

The three body part of the Skyrme interaction can be obtained as

$$
\begin{aligned}
\sum_{j,k;i\neq j\neq k} V^{(3)}_{ijk} &= \sum_{j,k;i\neq j\neq k}\int f_i(\mathbf{r}_i,\mathbf{p}_i,t)f_j(\mathbf{r}_j,\mathbf{p}_j,t)f_k(\mathbf{r}_k,\mathbf{p}_k,t)V(\mathbf{r}_i,\mathbf{r}_j,\mathbf{r}_k)\\
&\quad\times d^3r_i d^3r_j d^3r_k d^3p_i d^3p_j d^3p_k,\\
&= \sum_{j,k;i\neq j\neq k}\int f_i(\mathbf{r}_i,\mathbf{p}_i,t)f_j(\mathbf{r}_j,\mathbf{p}_j,t)f_k(\mathbf{r}_k,\mathbf{p}_k,t)t_2\\
&\quad\times\delta(\mathbf{r}_i-\mathbf{r_j})\delta(\mathbf{r}_i-\mathbf{r}_k)d^3r_i d^3r_j d^3r_k d^3p_i d^3p_j d^3p_k,\\
&= \frac{t_2}{(2\pi L)^3\cdot 3^{3/2}}\sum_{j,k;i\neq j\neq k} e^{-\left[(\mathbf{r}_i-\mathbf{r}_j)^2+(\mathbf{r}_i-\mathbf{r}_k)^2+(\mathbf{r}_k-\mathbf{r}_j)^2\right]/6L},\\
&= \frac{t_2}{(2\pi L)^3 3^{3/2}}\sum_{j,k;i\neq j\neq k} e^{-\left[(\mathbf{r}_i-\mathbf{r}_j)^2+(\mathbf{r}_i-\mathbf{r}_k)^2\right]/6L\times\frac{3}{2}},\\
&= \frac{t_2(4\pi L)^{3/2\times 2}}{(2\pi L)^3\cdot 3^{3/2}}\left[\sum_{j\neq i}\frac{1}{(4\pi L)^{3/2}}e^{-(\mathbf{r}_i-\mathbf{r}_j)^2/4L}\right]^2,\\
&= \frac{t_2 2^3}{3^{3/2}}\left[\sum_{j\neq i}\rho_{ij}\right]^2. \qquad (2.21)
\end{aligned}
$$

From the above derivation, one can observe that the three-body term reduces to two-body term. The finite range Yukawa term V^{Yuk} and an effective Coulomb intercation V^{Coul} are also included to account for various effects, therefore, read as:

$$V^{Yuk} = \sum_{j;i\neq j} t_3\frac{e^{-|\mathbf{r}_i-\mathbf{r}_j|/\omega}}{|\mathbf{r}_i-\mathbf{r}_j|/\omega}, \qquad (2.22)$$

$$V^{Coul} = \sum_{j;i\neq j}\frac{Z^2_{eff}e^2}{|\mathbf{r}_i-\mathbf{r}_j|}. \qquad (2.23)$$

With the inclusion of Yukawa term (with t_3 = -6.66 MeV and ω (range of Yukawa potential) = 1.5 fm), the surface properties of the nuclei are greatly improved. For the case of constant nuclear matter density, both interactions i.e., the two-body Skyrme as well as Yukawa interactions vary linearly with (ρ/ρ_0), whereas, the three-body part of the Skyrme interaction is proportional to $(\rho/\rho_0)^2$. In nuclear matter, the local potential energy has the form:

$$V^{Sky} = \frac{\alpha}{2}\left(\frac{\rho}{\rho_0}\right) + \frac{\beta}{\gamma+1}\left(\frac{\rho}{\rho_0}\right)^2. \tag{2.24}$$

The above equation contains α, β and γ as free parameters. α and β can be fixed by the general properties of the normal nuclear matter density such as the average binding energy should be -15.75 MeV and total energy should have a minimum at ρ_0. Further to probe the effect of different incompressibilities $K = 9[\rho^2 \frac{\partial^2}{\partial \rho^2}(\frac{E}{A})]_{\rho=\rho_0}$, the above equation is generalized to:

$$V^{Sky} = \frac{\alpha}{2}\left(\frac{\rho}{\rho_0}\right) + \frac{\beta}{\gamma+1}\left(\frac{\rho}{\rho_0}\right)^\gamma. \tag{2.25}$$

This equation expresses the nuclear equation of state and links pressure and energy [35, 208]. Also, it has been reported in Ref. [35] that the energy of the equation of state can be divided into compressional and thermal parts. Depending on the different values of the parameter γ, one can generate different equations of state. Obviously, higher value of γ corresponds to stiffer equation of state whereas, lower value of γ leads to softer equation of state. A detailed list of these parameters [used in Eq.(2.25)] corresponding to different equations of state is given in Chapter 4. The total Skyrme potential can be written as

$$V^{Sky} = \sum_{j;i\neq j} t_1\ \delta(\mathbf{r}_i - \mathbf{r}_j) + t_2\ \delta(\mathbf{r}_i - \mathbf{r}_j)\rho^{\gamma-1}((\mathbf{r}_i + \mathbf{r}_j)/2). \tag{2.26}$$

The above equation represents two terms, one is linear in density and it corresponds to the attractive term of Skyrme interaction whereas, the other term which gives power law dependence ($\propto \rho^2$) corresponds to the repulsive term of the same interaction. Also, it is worth mentioning that the above equation of state represents a cold matter. It is very much clear that matter resulted in a collision isn't only compressed, but is also hot. Due to this, Puri *et al.* [177] put forward temperature dependence of the mean field.

On incorporating the momentum-dependent potential, one has to again refit parameters of Skyrme force and their values have to be readjusted in such a way that same incompressibilities (as that of static equation of state as well as the ground state properties

of the normal nuclear matter) is reproduced. The parameterized form of the momentum-dependent potential, fitted to experimental data, is given as:

$$V_{ij}^{MDI} = t_4\ \ell n^2[t_5(\mathbf{p}_i - \mathbf{p}_j)^2 + 1]\ \delta(\mathbf{r}_i - \mathbf{r}_j), \tag{2.27}$$

where, t_4 and t_5 are, respectively 1.57 MeV and $5{\times}10^{-4}$ MeV^{-2}. A detailed discussion of the momentum-dependent interaction is also given in Chapter 4. The total baryon-baryon potential V_{ij} can be given as:

$$\begin{aligned} V_{ij} &= V_{ij}^{Sky} + V_{ij}^{Yuk} + V_{ij}^{Coul} + V_{ij}^{MDI} \\ &= t_1\ \delta(\mathbf{r}_i - \mathbf{r}_j) + t_2\ \delta(\mathbf{r}_i - \mathbf{r}_j)\rho^{\gamma-1}((\mathbf{r}_i + \mathbf{r}_j)/2) \\ &\quad + t_3\ \frac{e^{-|\mathbf{r}_i - \mathbf{r}_j|/\omega}}{|\mathbf{r}_i - \mathbf{r}_j|/\omega} + \frac{Z_{eff}^2 e^2}{|\mathbf{r}_i - \mathbf{r}_j|} \\ &\quad + t_4\ \ell n^2[t_5\ (\mathbf{p}_i - \mathbf{p}_j)^2 + 1]\ \delta(\mathbf{r}_i - \mathbf{r}_j). \end{aligned} \tag{2.28}$$

2.2.4 The nucleon-nucleon binary collisions

During the course of propagation, two nucleons can collide if they come close to each other and thus, scatter elastically or inelastically. The scattering of these nucleons is followed by a *Monte-Carlo* procedure which is Stochastic in nature and hence, is different from the Rutherford's scattering. In the QMD model simulations, we only consider binary collisions. Any two nucleons experience scattering if they come closer than a distance $\sqrt{\frac{\sigma^{free}(\sqrt{s})}{\pi}}$. This scattering is further subjected to the fulfilment of Pauli-principle. This means that if final state of scattered nucleons violates the Pauli-principle, the collision is said to be blocked. Here, $\sigma^{free}(\sqrt{s})$ represents the total free nucleon-nucleon cross-section and '$\sqrt{s}$' is the center of mass energy given below. The employed cross-section in the QMD model has been parameterized by Cugnon [209] using the experimental data. Here, different nucleons interact with the same cross-section without taking isospin degree of freedom into consideration. The total cross-section ($\sigma^{free}(\sqrt{s})$) is the sum of the cross-sections for elastic and inelastic channels. For the case of elastic channels NN$\rightarrow$NN, the total and differential cross-section (labeled as σ^{el}) is given as:

$$\sigma^{(el)}(\sqrt{s}) = \begin{cases} 55(mb) & \text{if}\sqrt{s} < 1.8993 \\ \frac{35}{1+100(\sqrt{s}-1.8993)} + 20 & \text{if}\sqrt{s} \geq 1.8993, \end{cases} \tag{2.29}$$

here, $(\sqrt{s})$, the nucleon-nucleon center of mass energy is given by:

$$\sqrt{s} = \sqrt{(E_1 + E_2)^2 - (\mathbf{p}_1 + \mathbf{p}_2)^2}. \tag{2.30}$$

where, E_i and $\mathbf{p}_i$ (i, j = 1, 2) are the energy and momentum of nucleon, respectively. For these elastic channels, the angular distribution is given by:

$$\frac{d\sigma^{el}}{d\Omega} \sim exp(T(s).k), \tag{2.31}$$

where, 'k' is squared momentum transfer and T(s) can be calculated from $\sqrt{s}$. On the other hand, for the case of inelastic channels NN→NΔ, the total cross-section (labeled as σ^{in}) is parameterized as:

$$\sigma^{(in)}(\sqrt{s}) = \begin{cases} 0 & \text{if} \sqrt{s} < 2.015 \\ \frac{20(\sqrt{s}-2.015)^2}{0.015+(\sqrt{s}-2.015)^2} & \text{if} \sqrt{s} \geq 2.015. \end{cases} \tag{2.32}$$

The angular distribution for inelastic channels is assumed to be isotropic. Depending on the fact that the mass of two nucleons is roughly equal to 1.876 GeV sets the limit of $\sqrt{s}$ = 1.8999 GeV [in Eq. 2.29]. Therefore, for two colliding nucleons with very small velocity, a constant cross-section (= 55 mb) is used. The mass limit for the inelastic channel [i.e., Δ formation in Eq. (2.32)] is based on the fact that the mass of Δ (= N + π) is 1.076 GeV. Therefore, for NN → NΔ channel, the outgoing mass should be at least (1.076 + 0.938) GeV. We shall discuss the detailed behavior of various isospin-dependent (i.e., energy and density dependent) and isopsin independent nucleon-nucleon cross-sections in Chapter 5. Further, above scattering is also subjected to the fulfilment of the Pauli-principle as it is a very important quantum feature. For the implementation of the Pauli-principle, it is assumed that each nucleon occupies a sphere in the coordinate and momentum space [35, 189]. The Pauli-blocking calculated with the help of this method gives the same results as that of an exact calculations of the overlap of Gaussians. The fractions P_1 and P_2 of the final phase space is calculated for each of the scattering partners. For simplicity, the binary nucleon-nucleon collision is blocked with a probability

$$P_{block} = 1 - [1 - min(P_1, 1)]\,[1 - min(P_2, 1)]\,, \tag{2.33}$$

and is allowed with probability = (1 - P_{block}) One obtains an average blocking probability (P_{block}) = 0.96 for a nucleus in its ground state. For absolute blocking, this factor should be unity. Thus, it is clear from the above discussion that Pauli-blocking will be zero or unity depending on whether the final phase space is occupied or not. It should be noted that this sharp occupancy is valid for the cold nuclear matter only. Puri *et al.* [177] also included the temperature by smearing the Fermi spheres for Pauli operator using

relativistic G-matrix. The input of in-medium corrections is found to be significant at low incident energies whereas, it washes at higher incident energies. Thus, as the incident energy increases, these effects will wash out and hence, the in-medium nucleon-nucleon cross-section approaches the free nucleon-nucleon cross-section. Also, hike in the incident energy leads to the velocity of nucleons comparable to the velocity of light demanding a complete covariant theory.

2.2.5 Other versions of the Quantum Molecular Dynamics model

During the recent years, a lot of efforts have been made by various research groups around the world to refine and modify the original QMD model [180–183]. The versions that are capable of handling low incident energies are Binding Quantum Molecular Dynamics BQMD [178], Pauli Quantum Molecular Dynamics (PQMD) [179], Extended Quantum Molecular Dynamics (EQMD) [171], Improved Quantum Molecular Dynamics (ImQMD) [172, 173], Fermionic Molecular Dynamics (FMD) [176] models etc. On the other side, the extensions like Relativistic Quantum Molecular Dynamics (RQMD) [180, 181], Ultra Relativistic Quantum Molecular Dynamics (UrQMD) [182–185] models etc. are designed to describe reactions at high and ultra high incident energies. A brief overview of these refined versions of the QMD model is given below.

2.2.5.1 BQMD model

To study the low energy fragmentation data, Bohnet *et al.* [178] made several changes in the structure of the original QMD model to make it suitable for low energy fragmentation data. This new approach was dubbed as "BQMD model" because it was designed to describe the proper binding of a nucleus in order to describe the phenomena of fragmentation [137, 210]. In addition, an improvement over stability against artificial particle evaporation was also achieved in the BQMD model. Here, nucleons are distributed within a sphere with Woods-Saxon-type density profile which is contrary to the original QMD model, in which, a sphere is used for the distribution of the centroid of Gaussians. Also, here maximum Fermi-momentum is limited by the local binding energy of the nucleons to keep all the particles bound and this is consistent with the original QMD model. Like in the standard QMD model, it also uses nucleons and deltas. The binary nucleon-nucleon cross-section was, however, kept isospin independent.

2.2.5.2 PQMD model

Peilert *et al.* [179] incorporated the Pauli-potential in the original QMD model and developed the PQMD model. They used the Gaussian Pauli-potential, proposed by Dorso *et al.*, [211]. The thermostatic properties of the system were obtained by averaging over several hundred statistically distributed manifestations and were sampled using Metropolis procedure [212]. On the basis of the appropriate cannonical weight, Pauli-potential is effective in the momentum and configuration spaces and thus, doesn't allow two identical particles to come very close to each other. The PQMD model has been successfully used to compare the FOPI data at low energies [213].

2.2.5.3 TQMD model

The Temperature-dependent Quantum Molecular Dynamics (TQMD) model incorporates temperature-dependent mean field potential among nucleons and is another realization of the standard QMD model. This model was put forward by Puri *et al.* [90, 177]. In original QMD simulations, one first calculates the so called local temperature at the position of i^{th} particle in each time step and then use this temperature to get the temperature-dependent potential which is finally used in the equation of motion. In principle, temperature should be defined at thermal equilibrium. It is worth mentioning that in intermediate energy heavy-ion reactions, no complete thermal equilibrium is reached. Puri *et al.* [177] gave a method to extract a reasonable defined temperature T, which is an extension of the usual definition in the thermal equilibrium using a local density approximation obtained from the simulations of heavy-ion collisions. The temperature dependent potentials used in the model were obtained by solving Bethe-Goldstein equation for the relativistic force in nuclear matter at finite temperature. The effect of temperature-dependent potentials was more pronounced in heavier masses compared to lighter masses [90, 177].

2.2.5.4 ImQMD model

Wang *et al.* [172, 173] incorporated many improvements in the original QMD model such as the surface and symmetry energy terms in the potential part and put forward the Improved Quantum Molecular Dynamics (ImQMD) model. This model has been successfully used to study the detailed dynamics of heavy-ion fusion at energies near the barrier. In this model, the wave packet width is taken as system mass dependent.

Also, phase space occupation constraint is considered for an approximate treatment of the antisymmeterization and used an isospin-dependent NN scattering cross-section which obeys the Pauli blocking [214]. In addition, an updated version of the ImQMD model i.e., the ImQMD-II [173] has been developed which incorporates the newly proposed Skyrme forces such as SkM* and and SLy series to study the properties of exotic nuclei in addition to stable nuclei. Further, to study the fusion reactions and halo-nuclei induced reactions as well as fusion dynamics for synthesizing super-heavy nuclei, the IQMD model was also modified by taking into account the shell effects and switch function method [215]. We have also compared the already published results using the ImQMD model with our calculated results (using the IQMD model [189]) and the comparisons are shown in Chapter 3.

2.2.5.5 FMD model

In this approach, the crucial quantum features like the antisymmeterization of the wave function was taken into account and is named as Fermionic molecular Dynamics (FMD) model [176]. In the initialization process of the QMD type models, the initialized nuclei are not really in their ground state with respect to the Hamiltonian used for their propagation. This drawback of the QMD model was taken care in this new approach i.e., FMD, developed by Feldmeier *et al.* [176].

2.2.5.6 AMD model

Ono *et al.* [174, 175] succeeded in developing the antisymmetrical version of the molecular dynamics model dubbed as Antisymeterized Molecular Dynamics (AMD) model. The selection of the width parameter which is taken dynamical in FMD is different than that taken in the AMD model, where it is constant. The FMD approach has been restricted by neglecting the time variation of the width parameter and that of spin wave functions [216]. So, by doing this, it becomes possible to treat many-nuclear systems. But the main drawback of this approach is that total angular momentum isn't conserved and thus, nucleon-nucleon collisions and therefore, the calculated values of the spins of AMD fragments may not be so reliable. To know more about this model along with the achievements in the development of the nuclear theory research, reader is referred to Ref. [175].

2.2.5.7 RQMD model

Faessler and co-workers [180, 181] modified the original QMD model to work up to relativistic energies and a new approach was put forward named Relativistic Quantum Molecular Dynamics (RQMD). The following improvements have been done over the original QMD model [180, 181, 217]:

- covariant dynamics has been taken and;
- an improved and extended collision term containing heavy baryon-resonances, strange particles and string-excitation for high energy hadron-hadron interactions has been incorporated.

The classical covariant equations of motion have been taken to study the time evolution of a many-body system. The many-body system moves in a $8\acute{N}$-dimensional phase with $6\acute{N}$ degrees of freedom; representing the classical configuration and momentum space. The time and energy of each particle is constrained in remaining $2\acute{N}$ degrees of freedom. The necessity of using an $8\acute{N}$-dimensional phase space is on the basis of no-interaction theorem (NIT) given by Curri *et al.* [218].

The RQMD model gives the same results as that of non covariant QMD model in the non-relativistic energy limit whereas, significant difference (between QMD and RQMD) appears at higher energies.

2.2.5.8 UrQMD model

The development of ultra-relativistic Quantum Molecular Dynamics (UrQMD) model [182–185] was reported by the *Frankfort group*. It has been further improved [219] by incorporating momentum dependence, Pauli-potential, in-medium NN→NΔ angular distribution and clusterization procedure. This modified version has the ability to explain the reaction mechanism over wider incident energy range from SIS ($\simeq$ 1GeV/nucleon) up to SPS ($\simeq$ 200 GeV/nucleon). Also, it can be used at even higher energies achieved in Relativistic Heavy Ion Collider (RHIC) or Large Hadron Collider (LHC). One can also use this approach to study the behavior of nuclear symmetry energy as well as its density dependence at densities very much above the normal nuclear matter density. But presently, we are only interested in the various phenomenon linked to intermediate energies where relativistic effects don't play much role [220].

2.3 Models used in the investigation of heavy-ion collisions with isospin effects

One of the major improvements over QMD model was to incorporate isospin degree of freedom. As it has been discussed in the Chapter 1, the Bethe-Weizsäcker mass formula introduced the idea of isospin, where symmetry energy term has been added to incorporate the asymmetry between neutrons and protons. Thus, first we shall introduce isospin-dependent Bolzmann-Uehling-Uhelenbeck (IBUU) model [186, 187]; which is very successful in explaining the role of the isospin in reaction dynamics and after that we will give details of the IQMD model, which has been used extensively to study reaction dynamics in the present thesis.

2.3.1 Isospin-dependent Bolzmann-Uehling-Uhelenbeck (IBUU) model

The IBUU model [186, 187] is a modified version of the original BUU model [221, 222] where the time evolution of the single particle phase-space distribution function is described by the Boltzmann-Uehling-Uhelenbeck equation:

$$\begin{aligned}\frac{\partial f_1}{\partial t} + v\cdot\nabla_r f_1 - \nabla_r U\cdot\nabla_p f_1 &= \int \frac{d^3p_1' d^3p_2 d^3p_2'}{(2\pi)^9}\sigma'_{12}v_{12}(2\pi)^3\delta^3(p_1+p_2-p_1'-p_2') \\ &\times\left[f_1' f_2'(1-f_1)(1-f_2) - f_1 f_2(1-f_1')(1-f_2')\right].\end{aligned} \tag{2.34}$$

In the above equation σ'_{12} and ν_{12} are differential cross-sections for a certain change of momentum $(\mathbf{p}_1\rightarrow\mathbf{p}_2)\rightarrow(\mathbf{p}_1'\rightarrow\mathbf{p}_2')$ and relative velocity for the colliding nucleons, respectively. The isospin degree of freedom has been incorporated in the model both by the elementary nucleon-nucleon cross-section σ^{IBUU} $(\sqrt{s})$ and the nuclear mean field 'U' (which is function of local density). The isospin dependence of the cross-section is taken in the model by assuming that the cross-section of neutron-proton (σ^{np}) is about three times that of neutron-neutron (σ^{nn}) and proton-proton (σ^{pp}) cross-section. The IBUU model gives an exact description of the time dependence of the one-body distribution function. An accurate solution of the BUU equation helps to wash out fluctuations in the density that might lead to the formation of fragments in an individual collision. The accurate solution of the BUU equation is generally achieved by solving the equation with

a large number of test particles per nucleon $\acute{N}_{test}$. Thus, in BUU calculations, the density fluctuations that lead to the fragment production are suppressed and hence, calculations of the fragment yield via the IBUU model isn't possible. Therefore, alternate models such as Stochastic Mean Field [188] and the IQMD [189] have been developed to address the density fluctuations.

2.3.2 Isospin-dependent Quantum Molecular Dynamics (IQMD) model

The IQMD model (based on the VUU code) is an extension of the QMD model (based on the BUU code). This model was developed by Hartnack *et al.* [189]. In the IQMD model, different charge states of nucleons, deltas and pions are treated explicitly. The isospin degree of freedom has been incorporated into the model via nucleon-nucleon scattering cross-section, Coulomb potential as well as symmetry potential (in the same manner as that in the IBUU model). Being an extension of the QMD model, it also consists of three steps viz; *Initialization*, *propagation* and *scattering*. But in all three steps, IQMD model behaves in a different way than the original QMD model [189]. For instance, during the process of initialization in the IQMD model, the centroid of the Gaussian in a nucleus are randomly distributed in a coordinate sphere of radius R=1.12A$^{1/3}$ corresponding to ground state density of $\rho_0 = 0.17$ fm^{-3}. Here, we have an option of taking large initial Fermi-momentum ($\mathbf{P}_F \simeq 270$ MeV/c) and it depends on the ground state density. Whereas, in the QMD model, the Fermi-momentum is determined by the local potential (using Thomas local Fermi-momentum approach), the Fermi-gas model is used to calculate the Fermi-momentum in the IQMD model. Since, momenta are uniformly distributed within a sphere, thus, nucleons close to the surface may be unbound initially. This results lesser binding energy of the initialized nuclei. On the other hand, with the availability of full Fermi-energy, a stronger density profile is achieved in the IQMD model. Another, major difference between the IQMD and the QMD model is the use of Gaussian-width 'L'; which measures the interaction range of nucleons. If we talk of the standard QMD model, 'L' is kept fixed, but on the other side, in the IQMD model, 'L' varies according to the size of the system i.e., 2.16 fm^2 for $^{197}_{79}$Au and 1.08 fm^2 for the $^{40}_{20}$Ca nucleus and in between these two limits for the masses lie between the mass of $^{40}_{20}$Ca and $^{197}_{79}$Au nuclei. This system size dependent of 'L' has been introduced to get maximum stability of the density profile of the given nucleus.

As given above, the IQMD model contains isospin terms of symmetry potential and Coulomb potential. In the QMD model, the effective charge is used for all nucleons without distinguishing between protons and neutrons whereas, in the IQMD model, one can have the real charge of the proton and neutron i.e., $Z_{proton} = 1$ and $Z_{neutron} = 0$ and hence, Coulomb potential is also isospin-dependent. In addition, the Yukawa potential is short ranged in IQMD model with its range $\omega = 0.4$ fm compared to $\omega = 1.5$ fm in the QMD model. Though, the potentials like Skyrme, Yukawa and momentum-dependent are independent of the isospin factor, the major ingredient of the IQMD model (incorporated in the QMD model) is the symmetry potential between protons and neutrons which has been described in Chapter 1. The behavior of the nuclear symmetry energy and its density dependence has been regarded as the most uncertain property of the isospin-asymmetric neutron-rich nuclear matter [223, 224]. Also, in addition to the density dependence of the nuclear symmetry energy, momentum dependence of the symmetry energy is one of the interesting topics in the present day nuclear physics research. Therefore, the IQMD model is different from the QMD model in terms of interaction potential 'U' and the total baryon-baryon potential in the IQMD model is given as:

$$\begin{aligned} V_{ij} &= V_{ij}^{Sky} + V_{ij}^{Yuk} + V_{ij}^{Coul} + V_{ij}^{MDI} + V_{ij}^{Sym} \\ &= [t_1\ \delta(\mathbf{r}_i - \mathbf{r}_j) + t_2\ \delta(\mathbf{r}_i - \mathbf{r}_j)\rho^{\gamma-1}((\mathbf{r}_i + \mathbf{r}_j)/2)] \\ &\quad + t_3\ \frac{e^{-|\mathbf{r}_i - \mathbf{r}_j|/\omega}}{|\mathbf{r}_i - \mathbf{r}_j|/\omega} + \frac{Z_i Z_j\ e^2}{|\mathbf{r}_i - \mathbf{r}_j|} \\ &\quad + t_4\ \ell n^2(t_5(\mathbf{p}_i - \mathbf{p}_j)^2 + 1)\ \delta(\mathbf{r}_i - \mathbf{r}_j) \\ &\quad + t_6\ (1/\rho_0)\ T_{3i}T_{3j}\ \delta(\mathbf{r}_i - \mathbf{r}_j). \end{aligned} \tag{2.35}$$

This is similar to Eq. (2.28), but the main difference in the mean field comes from the symmetry and Coulomb potentials. Also, here real charges are used in place of effective charge ($Z_{eff.}$), as used in the QMD model. The symmetry potential between protons and neutrons reads as:

$$V_{ij}^{Sym} = \sum_{j;i\neq j} t_6(1/\rho_0)\ T_{3i}T_{3j}\delta(\mathbf{r}_i - \mathbf{r}_j), \tag{2.36}$$

where, $t_6 = 100$ MeV and T_{3i} and T_{3j} represent the isospin projection of i^{th} and j^{th} particles (being +1/2 and -1/2 for protons and neutrons, respectively).

The total binding energy of a nucleus in its ground state is obtained from the expectation value of the total Hamiltonian. The kinetic energy, the Skyrme interaction and

the momentum-dependent interactions (MDIs) are analogous to the volume energy, the Yukawa interaction to the surface and the volume energy and the symmetry interaction to the volume symmetry energy when compared with Bethe-Weizsäcker mass formula. Also, it is important to mention that there is no term that corresponds to the pairing energy.

The parametrization of the nucleon-nucleon scattering cross-sections is different in the QMD and IQMD models. In the QMD model, NN collisions are governed by the Cugnon parameterization whereas, in the IQMD model, Verwest and Arndt parameterizations have been taken into account [225]. For the case of elastic NN collisions, the experimental parametrization has been adopted. Here, the treatment of the collisions is done in the same way as in the QMD model, but Pauli-blocking is isospin-dependent. This means that the occupancy of the phase-space of scattered partners is checked for the particles having same isospin as that of the scattered one. Not only nucleons and deltas (as formed in the QMD model), Pions are also formed via the decay of delta resonances.

The IQMD model has been used extensively to study large number of observables over wide range of incident energies [24, 29, 189, 226, 227]. Not only Hartnack *et al.* developed the IQMD model, two other groups have also done similar modifications over the original QMD model. In this direction, Chen *et al.* [228] have incorporated isospin degree of freedom in the QMD model and named it also Isospin-dependent Quantum Molecular Dynamics (IQMD) model. Here, in this approach, isospin dependence enters via mean field, binary nucleon-nucleon collisions and the Pauli-blocking, but it differs from the IQMD model developed by Hartnack *et al.* [189] in various aspects. For example, during the process of initialization of the projectile and target, the sample of neutrons and protons in the phase space are treated differently because of large difference between the neutrons and protons density distributions in nuclei far from the β-stability line. Also, interaction range (Gaussian width) is taken to be 2 fm^2 and kept fixed (i.e, independent of system size). Moreover, the range of the Yukawa potential is taken as 1.2 fm compared to 0.4 fm in the IQMD model developed by Hartnack *et al.* [189]. The experimental parameterization given by Chen *et al.* [228] is used for the isospin-dependent nucleon-nucleon scattering cross-section. Like the IQMD model developed by Hartnack *et al.* [189], here also, the total interaction potential is the sum of Skyrme, Yukawa, Coulomb, MDI and symmetry potentials and the details of these potentials are given in Refs. [189, 228]. This model has also been used to study the isospin dependence in fragmentation, collective flow etc. [117, 204, 229]. This model has been modified by incorporating the Pauli-potential and

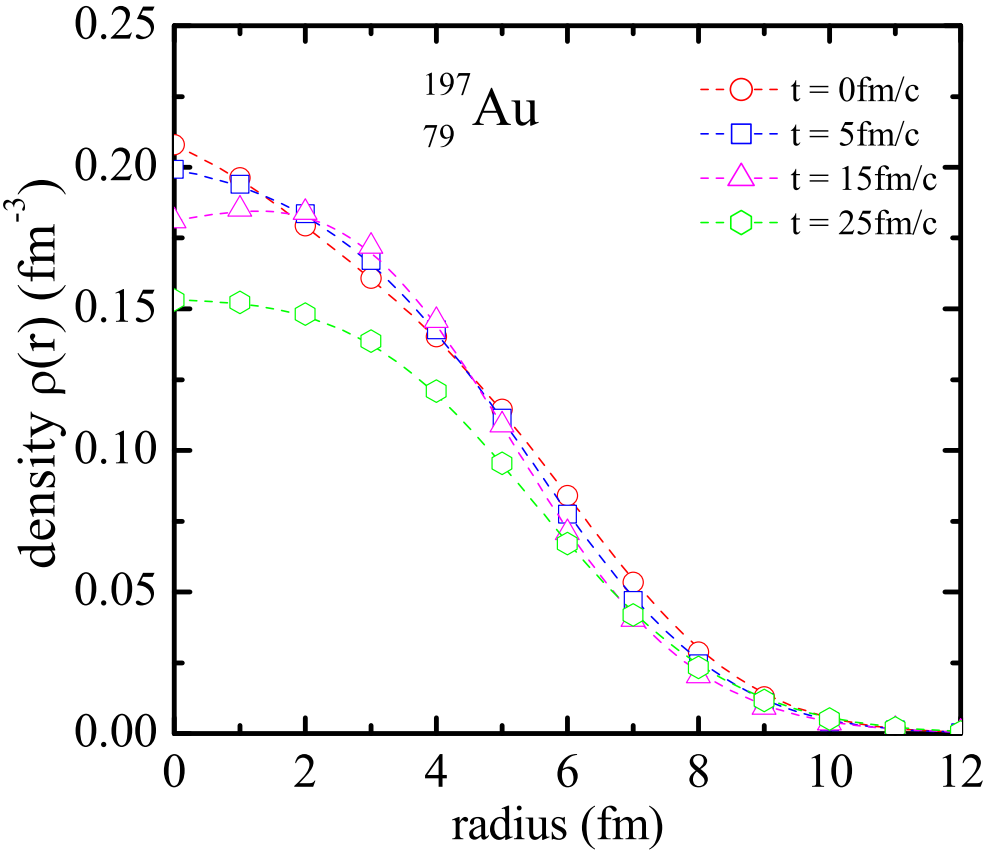

Figure 2.1: The time evolution of the density profiles ρ(r) obtained for the $^{197}_{79}$Au nucleus initialized within IQMD model using L=8.66 fm^2.

different forms of the symmetry potential (see Ref. [46] for details).

2.4 Numerical tests for the stability of nuclei generated in the IQMD model

Nuclei created in a transport model require various stability tests to check that if there is any spurious emission or not. For this, one requires to check initialization process

so that it doesn't destabilize the cold nuclei. Also, it is worth mentioning that once the interactions among the nucleons ceases to exit, then the formation of stable fragments takes place. *Heidelberg-Nantes-Frankfurt-tubingen-Chandigarh* groups have made extensive efforts to check the stability properties of different single nuclei. Before going in the details of the stability of initial nuclei in the IQMD model, it is important to shed some light on the Fermi-momentum taken in the IQMD model. As mentioned earlier, Fermi-momentum in the IQMD model is determined from the ground state density ($\rho_0 = 0.17$ fm^{-3}), evaluated using Fermi-gas model and its value comes about $\simeq$ 268 MeV/c. This value of Fermi momentum is different from the one taken in the QMD model, where its value is approximately equal to 150-160 MeV/c. Thus, the higher Fermi-momentum in the IQMD model leads to unbound nucleons at the surface (due to reduction in binding energy to 4-5 MeV/nucleon for heavy nuclei) and hence, may cause spurious emission. But at the same time, higher Fermi pressure leads to stronger stability of density profile and therefore stability of nucleus is preserved. Moreover, the interaction range in the IQMD model is also system size dependent to gain more stability of the density profile and ultimately, stable nucleus.

The time evolution of the density profile obtained in the $^{197}_{79}$Au nucleus using the IQMD model is displayed in Fig. 2.1 and one finds a stable shape at the surface. Also using broader Gaussian width (L = 8.66 fm^2) for the $^{197}_{79}$Au nucleus in spite of narrow Gaussian width (4.33 fm^2) leads to better stability of the shape of $r^2\rho(r)$ distribution [189] and therefore, motivated the choice of 'L' in the IQMD model.

Puri and co-workers have also carried out various stability checks by calculating the time evolution of the root mean square (r.m.s) radius and momentum of different nuclei [230]. For instance, the time evolution of r.m.s. radius and the momentum for four different nuclei ranging in the mass from $^6_3$Li to $^{197}_{79}$Au are displayed in Fig. 2.2. One can find that lighter nuclei (like $^6_3$Li) are little less stable whereas, for the heavy nuclei, there occurs the oscillations around the mean value, but no nucleons are emitted in the heavy-nuclei. It is worth mentioning that results are shown for 10 stable initializations. A small spurious emission in case of light nuclei (like $^6_3$Li) is because of the local density approximation isn't very good in light nuclei. Nevertheless, it has been found that majority of the nuclei remain stable for couple of hundred fm/c, which is long enough for the present calculations.

Another procedure for checking the stability is by plotting the phase-space distribution

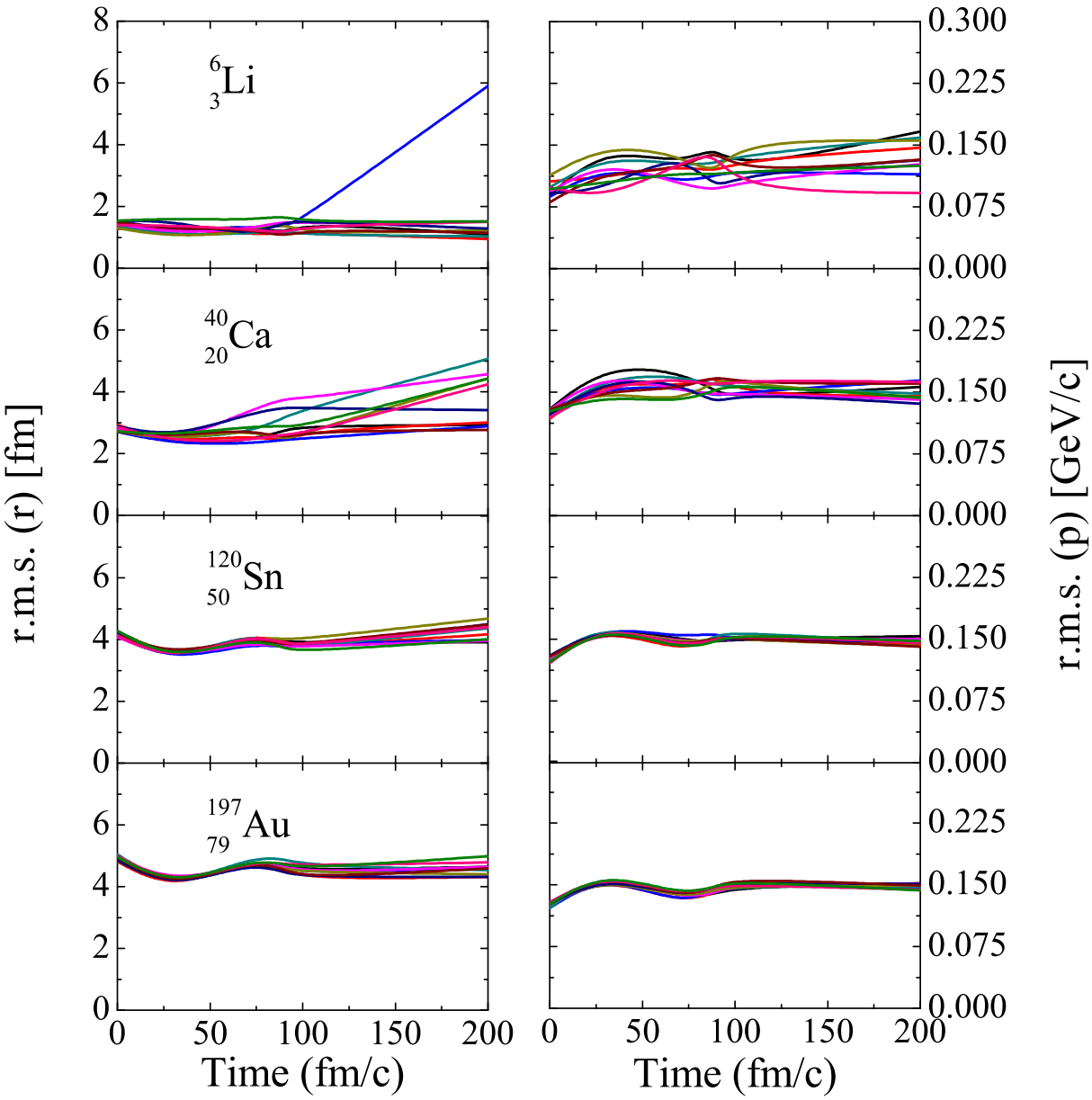

Figure 2.2: The time evolution of the root mean square radius in coordinate space (left panels) and momentum space (right panels). For each nucleus, we display the radius and momentum for ten different initializations. This figure is taken from the Ref. [230].

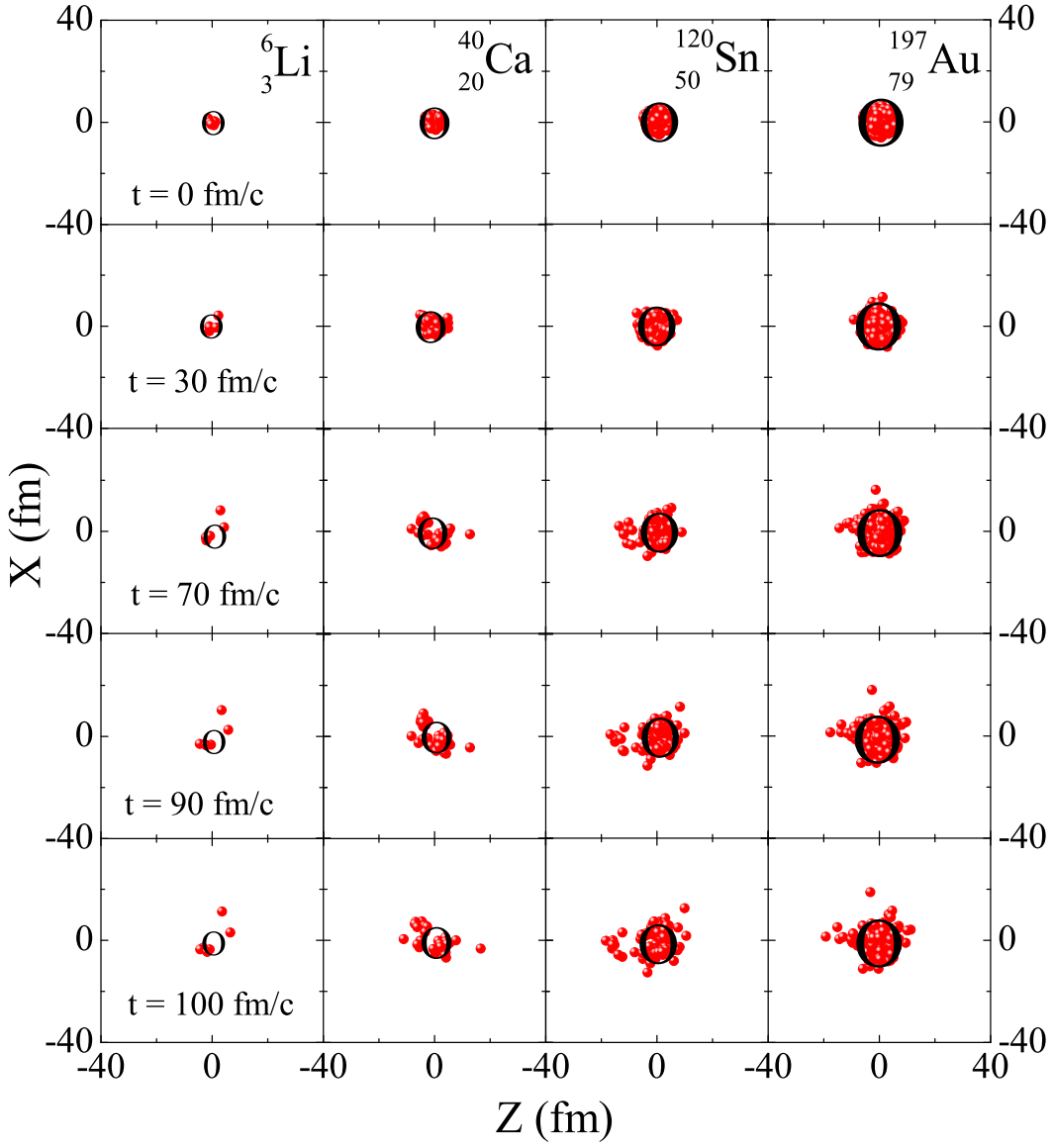

Figure 2.3: The phase-space distribution for four different nuclei in the co-ordinate space. This figure is taken from the Ref. [230].

of nuclei at different time steps. In Fig. 2.3, the phase space distribution of the four nuclei (ranging from $^{6}_{3}$Li to $^{197}_{79}$Au) at different time steps is shown. For better understanding, a circle of radius R = 1.12A$^{1/3}$ has also been marked. One can find that most of the nucleon remain inside the ellipse and few gets emitted in the time span of 200 fm/c and thus, indicates that nuclei are stable up to few hundred fm/c. Here, again, for lighter nuclei, approximation isn't good enough.

All the models discussed above are primary models that are mainly responsible for generating the phase-space of nucleons only. Further, there is also a need of "secondary models" to clusterize the nucleons into fragments. Some of the secondary clusterization methods are discussed briefly in the following section.

2.5 Secondary models for clusterization

The most extensively used phenomenology to clusterize the nucleons is the Minimum Spanning Tree (MST) method [24, 35, 203, 231–235]. In this method, two nucleons share the same fragment if their centroids are closer than a certain distance R_{clus},

$$| \mathbf{r}_i - \mathbf{r}_j | \leq R_{clus}, \tag{2.37}$$

where, $\mathbf{r}_i$ and $\mathbf{r}_j$ are the spatial positions of both nucleons. The value of R_{clus} can vary between $3 - 6$ fm. It has been reported that this range $(3 - 6$ fm) has small effect on the multiframentation process [235]. Also, we have shown the calculated results (in the Chapter 5) with $R_{clus} = 4$ fm and $\langle$3-6$\rangle$ fm and found that multifragmentaion is insensitive to the choice of the R_{clus} at freeze-out time of the reaction (freeze-out time of the reaction is the time where all motions and binary NN collisions cease to exist). At high density phase of the reaction, the MST method gives bigger fragments which further decays via the emission of several light and medium mass fragments after several hundred fm/c.

An improvement over the conventional MST algorithm, is to put additional constraint in momentum space. This method is called as MSTP [61, 203, 236]. This method also takes care of the relative momenta of nucleons. Along with the spatial constraint (used in the MST method), another constraint is put on the relative momentum of nucleons i.e.,

$$| \mathbf{p}_i - \mathbf{p}_j | \leq p_{min}, \tag{2.38}$$

where, p_{min} is of the order of average Fermi-momentum of nucleons. We have also shown the results for the yield of fragments by taking p_{min} = 200 MeV/nucleon in addition

to the default value (p_{min} = 268 MeV/nucleon) and it has been found that the yield of fragments is insensitive to an additional constraint of relative Fermi-momentum along with the spatial constraint (results are displayed in the Chapter 5).

In addition to the above secondary methods, an improvement over simple MST method is made by subjecting each pre-cluster to a constant binding energy constraint of - 4 MeV/nucleon. This method is dubbed as Minimum Spanning Tree with Binding energy (MSTB) [203, 237] Further, refinements have been made by taking binding energy formula, given by Samanta and Adikari [238] and by incorporating temperature-dependent binding energies. Puri and coworkers have also developed a new approach, dubbed as MST-BT [239]. Also Zhang *et al.* [235] improved the basic MST method by incorporating isospin degree of freedom and this improved method is called as iso-MST. This method leads to different spatial distances between proton-proton and neutron-proton for the formation of fragments.

In the same direction, Dorso and Randrup [240] gave an algorithm, namely, Early Cluster Recognition Algorithm (ECRA) and on the basis of this algorithm, Puri *et al.* [23] developed a novel clusterization algorithm known as Simulated Annealing Clusterization Algorithm (SACA). The SACA algorithm identifies the clusters at early stage of the reaction (i.e., 60-100 fm/c). Recently, the SACA model has been updated by Fevre *et al.* [241] to study the formation of hyper-nuclei and isotope yields in heavy-ion reactions. The modification has been done by including certain new features such as asymmetry energy, pairing energy and quantum effects and this new approach is dubbed as Fragment Recognition In General Application (FRIGA). In the present thesis, we will employ the basic MST and the MSTP secondary methods to recognize various fragments produced within IQMD model.

In summary, we have discussed the details of various primary and secondary models in this chapter. In the following chapters, we shall present our detailed studies for multifragmentation and associated phenomenon using stable and neutron-rich heavy-ion collisions. Our theoretical results are also compared with experimental data over the wide range of incident energy and colliding systems. Apart from this, isospin effects are also studied in the multifragmentation phenomenon in nearly symmetric and asymmetric reactions. All the calculations are carried out using IQMD model along with MST and MSTP algorithms.